PROCEEDINGS, 51st Workshop on Geothermal Reservoir Engineering
Stanford University, Stanford, California, February 9-11, 2026
SGP-TR-230

Evaluation of the Results of Distributed Temperature Sensing at the West Point Campus

Dante Fratta[1], James M. Tinjum[1], and David J. Hart[2]

[1]1415 Engineering Drive, Geological Engineering, University of Wisconsin–Madison, Madison, WI 53706, USA

[2]3817 Mineral Point Road, Wisconsin Geological and Natural History Survey, Madison, WI 53705, USA

Corresponding Author: fratta@wisc.edu

Keywords: distributed temperature sensing, thermal response test, borehole geophysics, fiber optics

Abstract:

We tested an exploratory 152-m geothermal borehole at a site in the United States Army Garrison, West Point, NY, as part of a Department of Energy (DOE) project to assess the site's geothermal potential. The test borehole site is located about 8.8 km southwest of the academic campus in the Hudson Highlands. The geology of these highlands comprises hard metamorphic rocks and shale, with igneous rock intrusions within a complex formation history and folding, as documented by borehole geophysics deployed at the site and cuttings examined during this field effort. A conventional thermal response test (C-TRT) at the site measured the composite thermal conductivity to be 2.82 W m^{-1} K^{-1}. To explore the vertical variability in the composite C-TRT thermal conductivity result, we also deployed a value-added optical Sensornet Distributed Temperature Sensing (DTS) interrogator to measure the temperature time history along the borehole depth. We instrumented the borehole with two multimode fiberoptic cables: one inside a 3.8-cm-inside-diameter HDPE circulation pipe and another outside the circulation pipe. The results allow evaluation of thermal conductivity with depth and the relationships between those parameters and different rock types and layers in the formation. Our DTS results indicated thermal conductivity values ranging from 1.3 to 3.6 W m^{-1} K^{-1}, both of which support the variability of thermal properties in metamorphized rocks and the range of values that depend on mineralogical content, dipping beds, faulting, and other features. These distributed results can guide the design of more efficient geothermal energy systems (e.g., optimal depth and spacing).

1. INTRODUCTION

The DOE Office of Geothermal and the Federal Energy Management Program (FEMP) created the Federal Geothermal Partnerships (FedGeo) initiative to expand geothermal heating and cooling efforts at federal sites nationwide. In addition, the DOE's Oak Ridge National Laboratory and collaborators provide data analysis, resource characterization, site surveys, and geothermal heat pump and district-scale geothermal system design for the sites. Collected datasets and interpreted results can help federal facilities assess whether to pursue geothermal systems. FEMP can then support the identification of the optimal financing mechanism for on-site project development.

The University of Wisconsin–Madison (UW–Madison) Geothermal and Energy Geotechnics Research Group was contracted by The National Laboratory of the Rockies (NLR)—a U.S. Department of Energy (DOE)-managed national laboratory dedicated to "energy systems innovation and integration, enhancing existing technologies, and developing new, cutting-edge solutions that unlock economic opportunity and fuel America's global competitiveness" (NLR 2026). As part of these efforts, UW–Madison collected data to determine the thermal and hydrogeological properties at a site in the United States Army Garrison West Point (USAG West Point) complex in southeastern New York. We determined the distributed subsurface thermal and hydrogeological properties at the sites, representing a variety and range of hydrogeological conditions. The expected outcomes include obtaining comprehensive distributed thermal-hydrogeological property measurements and conducting a technical-economic analysis of vertical bore geothermal heat exchange (GHE) installations at these sites. In future projects, we aim at quantifying the operational efficiencies of geothermal heat exchange and buildup—including the influence of groundwater movement and distributed geology, using borehole geophysical characterization, sentry and drawdown wells with piezometers, and distributed temperature sensing arrays are used to analyze whether a field can dissipate excess heat to the environment in addition to providing essential long-term data for health assessment, machine learning, and tuning of operational efficiencies.

2. BACKGROUND

At the test borehole site of USAG West Point, our research team was responsible for providing *in situ* characterization of the geothermal resource. We supported drilling activities, deployed geophysical techniques, installed advanced monitoring equipment, and examined the distributed thermal, physical, and hydrogeological properties and expected performance. These efforts inform the depth and spacing of a proposed borefield for future geothermal projects. At the same time, combined datasets serve as valuable input into techno-economic analyses and are used to site and size the appropriate geothermal fields.

In particular, we expanded on conventional thermal response test (C-TRT) results with distributed temperature-sensing (DTS) measurements along the depths of the tested borehole to provide valuable insights into effective borehole parameters. We advanced techniques to analyze the results of the fiber-optic distributed thermal response test (D-TRT) and to provide details on the variability of subsurface heat transfer along a borehole (e.g., showing where appreciable variation in subsurface heat flow exists). Gains in energy efficiency can be made by optimizing the design and layout of new geothermal borefields, which is the most expensive and variable

capital component of a ground heat exchange (GHE) system. This techno-economic evaluation will be informed by the characterization results, thereby optimizing borehole depth, spacing, and borehole-field layout.

2.1 Geology description at the testing site

In the summer of 2024, Brightcore Energy (Armonk, NY) drilled a ~150 m (with a typical 5.5 m horizontal deviation to the south) borehole at the test site of the United States Army Garrison, West Point, NY. This annex is located about 8.8 km (5.5 miles) southwest of the main academy campus in the Hudson Highlands. The geology of these highlands comprises a complex system of hard metamorphic rocks and shale, with igneous intrusions (e.g., gneiss and granite rocks) within a complicated formation history and folding. The bedrock encountered at the drilling site was primarily gneiss and amphibolite, with variations in mineral composition (Figure 1).

Johnson and Gellasch (2004) describe the geologic history of the metamorphic rocks of the Hudson Highlands. During the Middle Proterozoic, sedimentary rocks formed into an island arc, which was later deeply buried and metamorphosed into gneisses in the Late Proterozoic. Large-scale extension followed a mountain-building period during the Early Paleozoic, when sediments in the proto-Atlantic Ocean buried the gneisses and granites. In the Late Paleozoic, the proto-Atlantic Ocean closed, and the Hudson Highlands deformed in three stages from the Ordovician through the Permian, during which portions of the Hudson Highlands pushed westward (O'Brien 1987) and igneous rocks intruded. The Atlantic Ocean opened during the Mesozoic, and block faulting accompanied the breakup of Pangea. In the Cenozoic and Pleistocene periods, erosion exposed the rock, and glaciers further carved the landscape (Johnson and Gellasch 2004). The worldwide glaciation began 1.6 million years ago, and the Laurentide Ice Sheet covered nearly all of current-day New York State, around 21,750 years ago (Isachsen et al. 2000). Many glacial features were eroded before the glaciers eventually retreated around 10,000 years ago (Isachsen et al., 2000). The current-day geology for the region examined consists of layers of gneiss and amphibolite. The bedrock geology at the test borehole site is described as "Quartz plagioclase gneiss; may contain pyroxenes, hornblende, biotite; locally interlayered with amphibolite; subordinate biotite mesoperthite gneiss" (*Geological Map of New York, Lower Hudson Sheet* 1970).

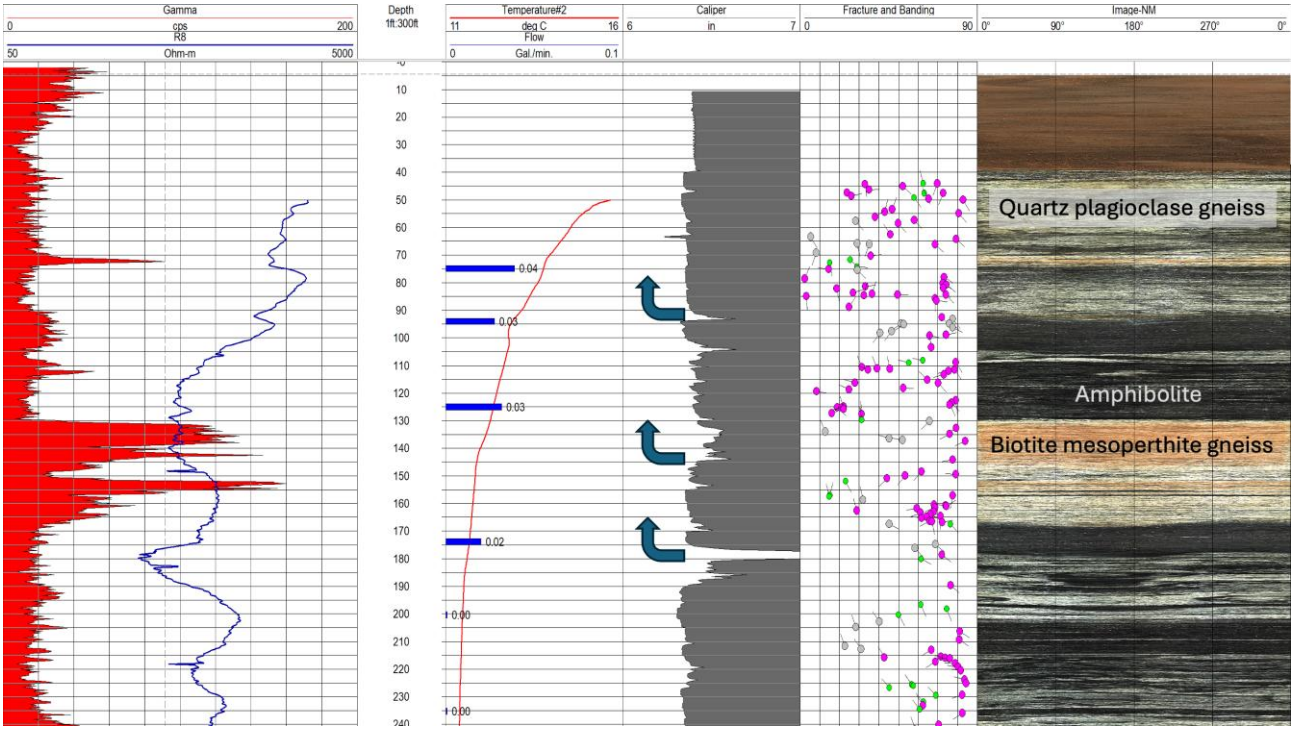

Figure 1: Geophysics logs at the test borehole site. The red and blue lines in the left column are the results of downhole geophysical gamma-ray logging and electric resistivity logging, respectively. The red line in the central column of the figure shows the downhole temperature, and the blue bars in the central column show groundwater flow from fractures at those depths. The gray logging to the right of the temperature and groundwater flow measurements is the caliper reading, showing variation in borehole diameter with depth. The pink, gray, and green dots in the second-to-last column on the right represent fractures and bedding features identified throughout the boring. The location of the dot, plotted between 0° and 90°, is the dip angle of each of these features, with the line connected to each of the dots pointing in the azimuth of the strike direction. The gray dots represent a filled fracture/joint, the green dots represent bedding/banding/foliation, and the pink dots represent a minor open joint/fracture. The downhole camera image of the boring is shown on the far right.

The thermal conductivity for gneisses generally ranges between 1.7 and 5.7 W m^{-1} K^{-1} (Kavanaugh et al. 1997, Walker et al. 2015), depending on the mineral composition of the gneiss, as well as on fractures and water content. The thermal conductivity of amphibolite

ranges between 2.2 and 2.7 W m^{-1} K^{-1} (Pribnow et al. 1996), with variations dependent on saturation level and temperature. Based on the variations of mineral composition throughout the stratigraphy encountered at the borehole, the thermal conductivity for the gneiss and amphibolite layers is expected to fluctuate within this range.

2.2 Ground-coupled heat pump systems

Ground-Coupled Heat Pump (GCHP) systems use thermal energy stored in the Earth as an environmentally friendly, operationally low-cost source for space heating and cooling (Ozenger et al. 2006, Chua et al. 2010). Depending on the season and facility requirements, GCHP can be substantially more efficient than using ambient air as a heat source or sink. This is because most ground temperatures are warmer than the ambient air in winter and cooler in summer, improving the efficiency of heat pumps used for space heating and cooling. The temperature fluctuates in the shallow subsurface (<10 m deep) due to atmospheric interactions, whereas at greater depths (>50 m) the subsurface temperature approaches the natural geothermal gradient (Grant et al. 1982, Ozdogan-Dolcek et al. 2014).

GCHP systems use a carrier fluid to circulate the heat between the GHX borefield and the heat pump, and most GHXs are constructed with vertical boreholes. Vertical GHX systems typically consist of high-density polyethylene (HDPE) U-tubes placed into boreholes. The space between the U-tube and the borehole wall is generally filled with high-thermal-conductivity grout that improves thermal contact between the loop and the surrounding soil/rock and prevents groundwater cross-contamination of the aquifer. Typical boreholes have historically had depths of 40 m to 150 m and diameters of 0.075 m to 0.15 m (Diao et al. 2004), but building- and campus-scale systems are now evolving to much greater depths in an attempt to maximize the heat potential of medium to deep formations (Piipponen et al. 2022).

Geothermal exchange models and systems were initially intended for small facilities rather than for large buildings or campuses. So, special considerations must be taken into account in the design of commercial or district-scale GCHP systems, as the greater number of boreholes creates thermal interactions among them that are not accounted for in the GHX design for small facilities (IGSHPA 1991, Kavanaugh 1995, Fan et al. 2015). Furthermore, buildings on district-scale campuses are commonly cooling-dominant due to internal heat generation and data center functions, leading to overheating and reduced efficiency over time (Heeg et al. 2024, Knudson 2013, Yang et al. 2013, Zhou et al. 2014). Still, large-scale GCHPs offer a significant opportunity to save energy and reduce carbon emissions. Thus, if large GHX borefields could be reliably designed to operate efficiently in the long term, GCHP systems could become a preferred method for space heating and cooling large-scale facilities (Heeg et al. 2024).

Liu et al. (2019) report that GCHP system design tools and supporting data (e.g., geological characteristics and near-surface thermal properties) require improvements and higher sophistication to enable optimal design and integration. Responding to these calls, technological developments are leading to lower-cost, performance-neutral GHXs, more cost-effective GHX equipment and system configurations, and automated processes for the design and performance evaluation of such systems. For example, the DOE (2012) identified high first costs for the ground loop(s) and long-term temperature drift as significant roadblocks. Although several handbook, analytical, numerical, and hybrid models exist, borefields continue to exhibit significant operational performance degradation over time. Some of those models include the G-function model developed by Eskilson (1987) and the duct storage temperature (DST) model developed by Hellstrom (1989). The Eskilson (1987) method uses a normalized step-response function to define the relationship between the average borehole temperature and a step change in heat extraction or rejection for a pre-defined borehole geometry, while the Hellstrom (1989) method uses a combination of analytical and numerical methods.

2.3 Importance of Subsurface Geology for GCHP Design

The geology of a GHX field plays a vital role in its practical design and management. The loop design must account for heat transfer in the geology (IGSHPA 1991, Spitler 2005, Busby et al. 2009, ASHRAE 2011). Essentially, all GHX design approaches rely on λ_{ground} estimates. Geologies with higher thermal conductivities maximize heat transfer and minimize the loop size in GCHP systems (Diao et al. 2004, Fan et al. 2007, Dehkordi and Schincariol 2013, Hecht-Mendez et al. 2013). An extensive design effort is conducted to ensure the loop length is neither too short (resulting in exiting high water temperatures from the field) nor too long (resulting in first costs that are too expensive).

The ground is usually assumed to be homogeneous in thermal response testing analysis and with building energy design tools. However, the ground is commonly stratified with layers of geologic material of varying thermal properties and hydrogeological conditions. For example, in a comprehensive study of the thermal conductivity of rock formations in Wisconsin, thermal conductivity ranged from 1.84 to 6.71 W m-1 K-1, and specific heat ranged from 713 to 891 J kg-1 K-1 (Walker et al. 2015). Saturated rock conducts heat better than unsaturated rock (Horai and Simmons 1969, Zimmerman 1989, Clauser and Huenges 1995, Meyer 2013). The effect of ground heterogeneity on the performance of GHX systems has been understudied and remains uncertain. For example, McDaniel et al. (2018c) report that ground temperature profiles along boreholes can vary significantly due to lithological changes. Therefore, lithological changes along the length of GHX should be considered in any practical GHX design.

The number of boreholes and borehole depth are highly dependent on the $\lambda_{ground,}$ which, in turn, strongly influences initial borefield cost, particularly for commercial buildings (Yavuzturk 1999). Determination of λ_{ground}, however, is a significant challenge. Design methods do not account for variable ground thermal properties or the deep geothermal gradient. Further, and potentially of great importance, heat can also be carried away from the field by groundwater. A hydraulic gradient drives groundwater flow, moving most quickly through geology with high hydraulic conductivities. Dehkordi and Schincariol (2013), Walker et al. (2015), and Catolico et al. (2016) emphasized the importance of thermo-hydrogeological parameters, undisturbed ground temperature, and ground thermal

properties for GCHP design and performance. However, geothermal exchange software generally does not adequately provide the impact of groundwater flow.

3. MATERIALS AND METHODS

During June and July 2024, we deployed and interrogated Distributed Temperature Sensing (DTS) arrays to support the thermal characterization of the 152-m (500-ft) testing well drilled at the West Point Annex site. The DTS technique uses rapid-fire laser pulses into the silica fiber while monitoring the return signals from Raman backscattering events. We deployed three multimode fiber-optic cables and interrogated them with a Sensornet Halo DTS interrogator to monitor the well's thermal history during and after the thermal response test (TRT). We installed two fiber-optic cables at the site. One of the cables was run up and down the well, outside the HDPE pipe, for 304 m (1000 ft) (Figure 2). While the other cable was run up and down inside each leg of the HDPE pipe (Figure 3). Each fiber-optic cable was protected by a 9.5 mm (3/8 in.) OD diameter plastic tubing. The protective plastic tubing creates a delay in the fiber-optic temperature response, but it is not of consequence in slow heat transfer processes.

We deployed cold- and hot-water baths, monitored with thermocouples, to calibrate the optical responses and obtain temperature distributions along each fiber-optic run. The DTS interrogator, water baths (controlled by a circulating pump for the hot-water bath and a small refrigerator for the cold-water bath), a data logger, and a computer.

We collected data with four DTS interrogator channels using single-ended configurations. Channels 1 and 4 collected single-ended data by sending laser pulses to each end of the fiber, located outside the HPDE pipe. Each end of the fiber-optic cables was routed through the cold- and hot-water calibration baths to provide a more robust contrast for the calibration algorithm. Channels 2 and 3 collected data on single-ended configurations from each of the two fiber-optic cables within the HPDE pipes. The initial sections of each fiber-optic cable were placed in the cold and hot baths. Details of these configurations are documented in Figures 2 and 3, while Figure 4 documents the time history of calibration baths during the monitoring period.

During the monitoring period, the water bath temperatures were not constant (Figure 4). The thermocouples captured operational effects. For example, when the hot water bath fluctuated, we turned on and off the circulating pump to avoid bringing the cooler's temperature to high values (we wanted to avoid temperatures above 65 °C), and we periodically added ice to the cold-water bath to initially keep the water temperature close to 0 °C. Those sudden changes created difficulties during the calibration process as the Sensor net interrogator and the data logger for the thermocouple ran with independent clocks and uneven sampling intervals. In each water bath, we placed more than 8 m of fiber-optic cable, which was then used to calibrate the optical measurements collected with the DTS interrogator.

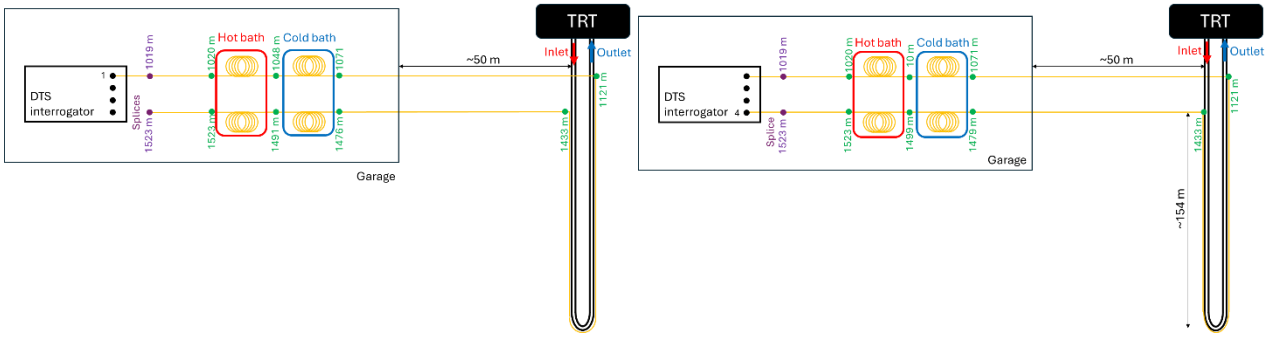

Figure 2. Distributed temperature sensing for channels 1 and 4. The fiber-optic cable ran outside the HDPE tube from the top to the bottom and back to the top of the well.

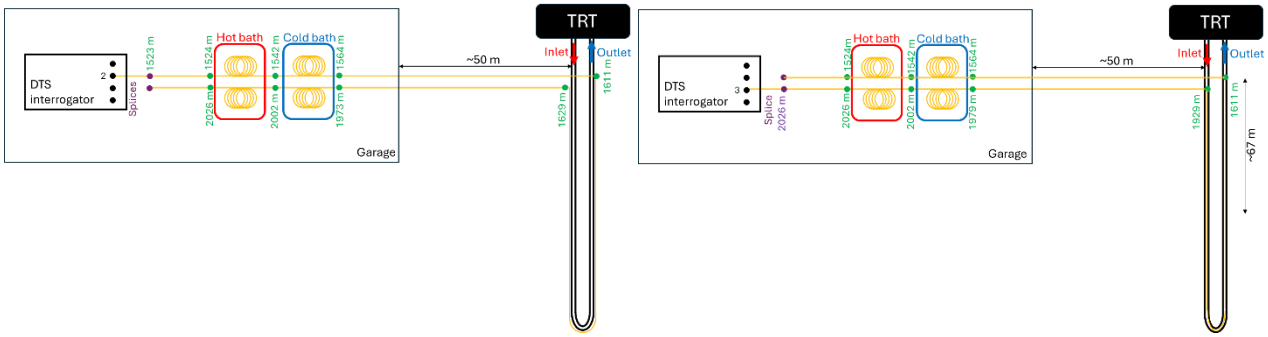

Figure 3. Distributed temperature sensing for channels 2 and 3. The fiber-optic cable ran inside the HDPE tube from the top to the bottom and back to the top of the well.

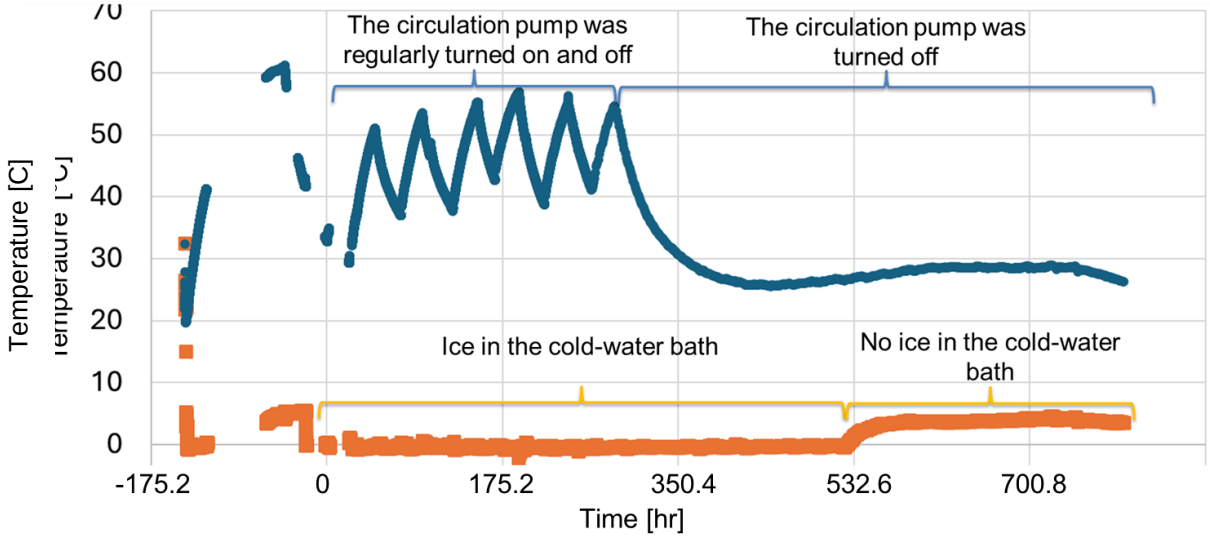

Figure 4: Time history of the temperature in the hot and cold-water baths. Changes in the temperature history reflect the on-and-off operation of the circulating pump in the hot-water bath and the addition of ice to the cold-water baths. Note: the calibration of the results is challenging due to using an external data logger with the DTS systems, uneven sampling rates during data logger data collection, rapid changes in the hot water baths, and different timestamps between the data logger and the DTS computers.

The DTS interrogator data are calibrated by determining parameters Δα, γ, and C for each measurement sequence in this equation (McDaniel et al. 2018a, 2018b):

$$T(z_i, t_k) = \frac{\gamma}{ln\left[\frac{P_S(z_i,t_k)}{P_{aS}(z_i,t_k)}\right] + C - z_i\Delta\alpha} \tag{1}$$

where $T(x_i,t_k)$ is the calibrated temperature at position z_i along the fiber at measurement time t_k, and $P_S(x_i,t_k)$ and $P_{aS}(x_i,t_k)$ are the Stokes and anti-Stokes Raman scattering responses at position z_i along the fiber at measurement time t_k given the DTS interrogator. To determine the Δα, γ, and C, we use the known temperatures $T(z_{wb},t_k)$ at the location of the z_{wb} of the hot and cold-water baths at all times, t_k. The parameters are found by rearranging Equation 1 for the water baths and implementing the least square solutions:

$$ln\left[\frac{P_S(z_{wb},t_k)}{P_{aS}(z_{wb},t_k)}\right] = \frac{\gamma}{T(z_{wb},t_k)} - C + z_{wb}\Delta\alpha \tag{2}$$

where $P_S(z_{sw},t_k)$ and $P_{aS}(z_{sw},t_k)$ are the Stokes and anti-Stokes Raman scattering responses at the water baths for all the measurement times. Equation 2 is rearranged as a matrix multiplication for each measurement time:

$$\begin{bmatrix} ln\left[\frac{P_S(z_1,t_k)}{P_{aS}(z_1,t_k)}\right] \\ \vdots \\ ln\left[\frac{P_S(z_T,t_k)}{P_{aS}(z_T,t_k)}\right] \end{bmatrix} = \begin{bmatrix} \frac{1}{T(z_{wb},t_k)} & -1 & z_{wb} \\ \vdots & \vdots & \vdots \\ \frac{1}{T(z_T,t_k)} & -1 & z_T \end{bmatrix} \cdot \begin{bmatrix} \gamma^{<k>} \\ C^{<k>} \\ \Delta\alpha^{<k>} \end{bmatrix} \tag{3}$$

where T is the number of measurements in the water baths. Rewriting it as a matrix multiplication, Equation 3 becomes:

$$y^{<k>} = L^{<k>} \cdot x^{<k>} \tag{4}$$

Where vector $y^{<k>}$ represents all the natural logs of all ratios of Stokes and anti-Stokes of the Ramman backscattering at times k, $L^{<k>}$ is the matrix of the coefficients for times k, and $x^{<k>}$ is the vector of each unknown parameter for times k. Then, the least squares solution to solve for the unknown parameters is at time k:

$$x^{<k>} = [(L^{<k>})^T \cdot L^{<k>}]^{-1} \cdot (L^{<k>})^T \cdot y^{<k>} \tag{5}$$

We applied this solution to all the data collected from the four DTS interrogator channels. Figure 5 compares the instrument-calibrated data with data calibrated using Equations 2-5. These results look very similar. However, Figure 6 shows a zoomed-in view of the results and documents that the sudden, abrupt changes in bath temperature are reflected in the calibration results. Overall, the long-term trends are similar (Figure 7). Still, sudden changes in bath temperature add noise to the calibrated temperature values.

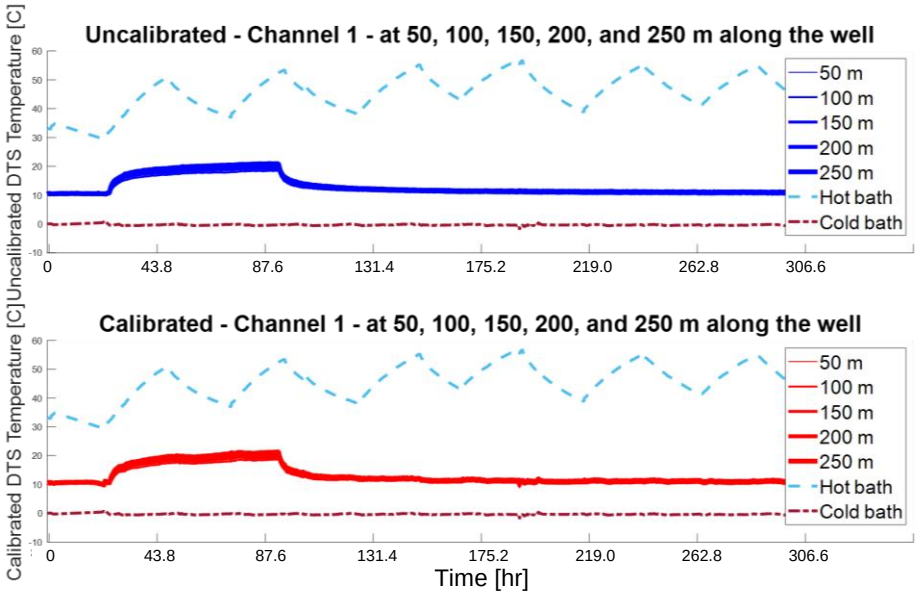

Figure 5: Comparison of DTS temperatures with the field-calibrated (i.e., uncalibrated) and post-calibrated (i.e., calibrated) temperatures.

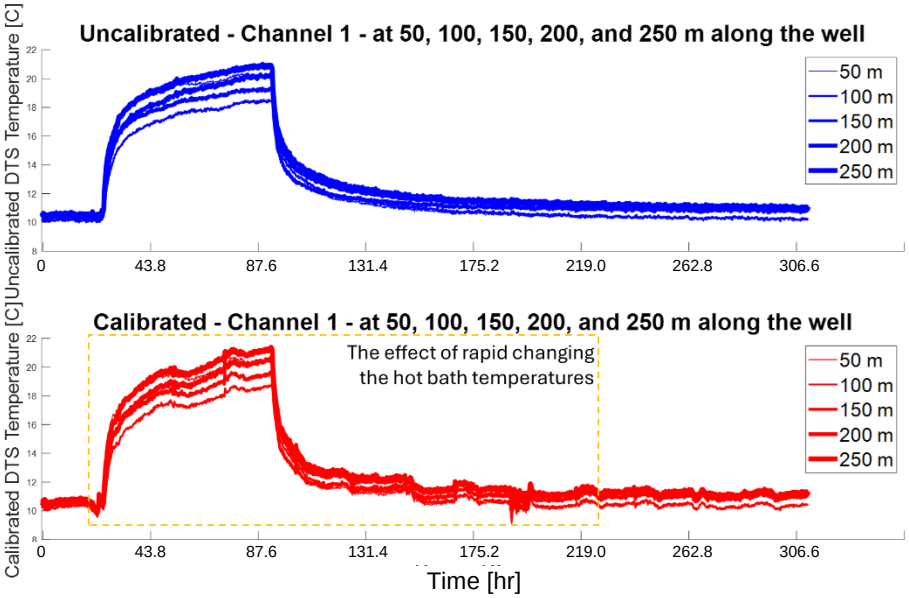

Figure 6: Effect of sudden changes in the calibration bath temperatures in post-calibrated (i.e., calibrated) temperature results.

4. RESULTS

The data collected at the borehole revealed correlations between geological formations and geophysical logs, confirming the presence of quartz-plagioclase gneiss, amphibolite, and biotite mesoperthite gneiss, as shown in the logging data (Figure 1). Fractures were identified at multiple depths; however, no significant fluid flow was detected, with only minimal flow observed under pumping conditions. We located transmissive fractures at depths of 31.7, 48.3, and 60.0 m that contributed a total flow of $2.5 \cdot 10^{-3}$ L s^{-1}. The horizontal deviation of the WP-TRT1 borehole was approximately 5.5 m to the south, a typical deviation for boreholes.

Cutting samples were collected at 1.5-m intervals, identified under a microscope, and analyzed for their mineralogical composition to estimate thermal conductivity (Luebbe 2025). The thermal conductivity of each mineralogical layer was calculated using both parallel and perpendicular methods, with porosity corrections applied to specific layers. The uncorrected thermal conductivity ranged from 4.00 to 5.38 W m^{-1} K^{-1}, with an average of 4.69 W m^{-1} K^{-1}. After using a thermal impedance correction factor, the adjusted thermal conductivity ranged from 2.40 W m^{-1} K^{-1} to 3.24 W m^{-1} K^{-1}, averaging 2.82 W m^{-1} K^{-1}. The D-TRT conducted at this site corroborated the adjusted results (see Analysis).

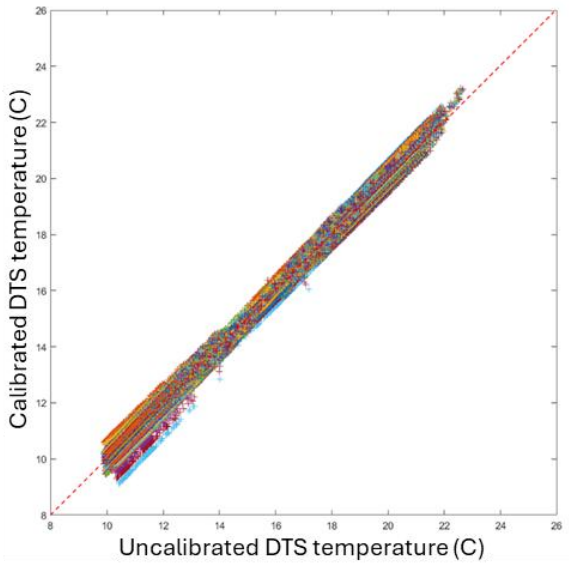

Figure 7: Overall long-term comparison of the field-calibrated (i.e., uncalibrated) and post-calibrated (i.e., calibrated) temperatures.

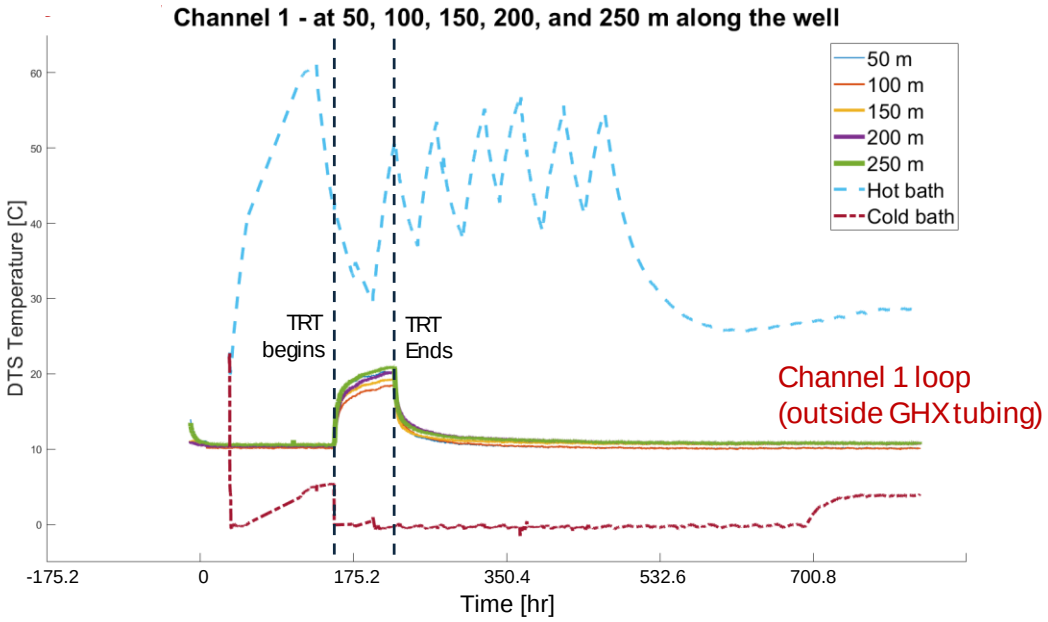

Figure 8: Summary of the temperature response of channel 1 before, during, and after the completion of the C-TRT test.

We deployed three multimode fiber-optic cables and interrogated them with a Sensornet Halo DTS interrogator to monitor the well's thermal history during and after a conventional thermal response test (C-TRT). During the C-TRT test, constant heat is added to the circulating water in the GHX pipe while the inlet and outlet temperatures are monitored. The interpretation of the C-TRT results yields average thermal parameters for the geological formation along the GHX pipe. The advantage of adding fiber optics and distributed temperature sensing to the GHX is that we collect data to invert for the distributed thermal properties, developing what we refer to as the distributed thermal response test (D-TRT).

Figure 8 summarizes the data collected by channel 1 before, during, and after the C-TRT at depths of 50 m, 100 m, 150 m, 200 m, and 250 m. Throughout the well, the DTS captures the temperature increase and dissipation during heat injection. Figure 9 presents the waterfall temperature plots of the calibrated temperatures for all four channels. Note the horizontal strikes in the color plots. These strikes are caused by differences in thermal properties across the formation. Some thermal responses lag behind the temperature increase, even though the heat power during the thermal response test remains constant. Finally, Figure 10 documents temperature

profiles during the heating phase of the C-TRT testing. These data are used to calculate the distribution of thermal conductivity along the formation length.

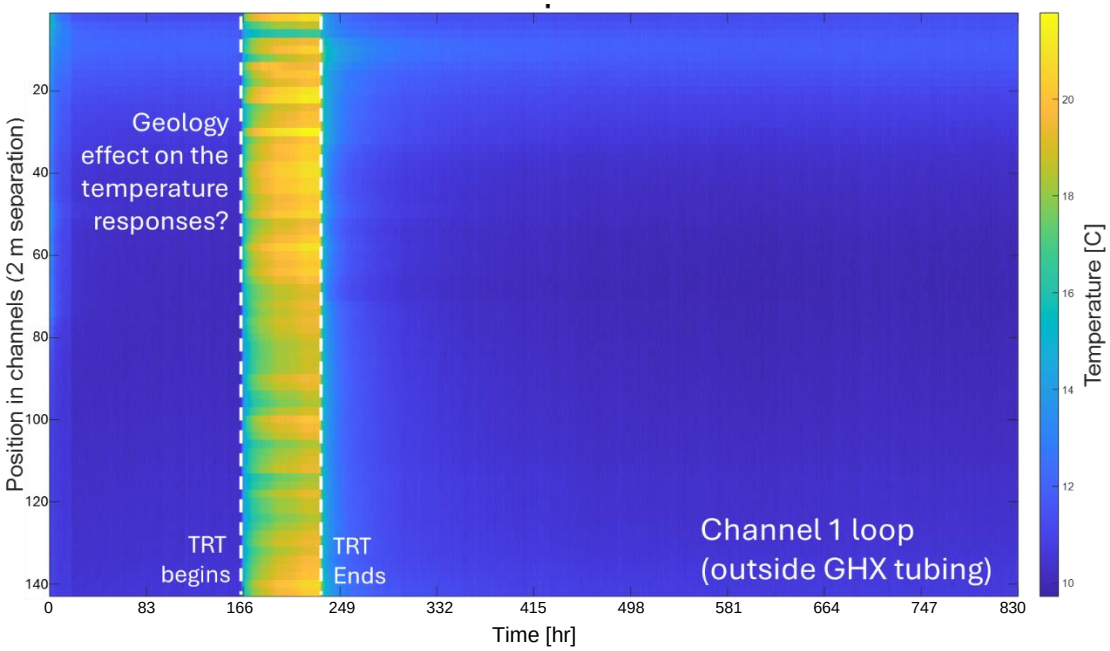

Figure 9: Waterfall plot of the temperature in the downward leg of channel 1 before, during, and after the completion of the C-TRT test. Please note how the geology's heterogeneity appears to influence the well's heating and cooling if the grouting property is constant with depth.

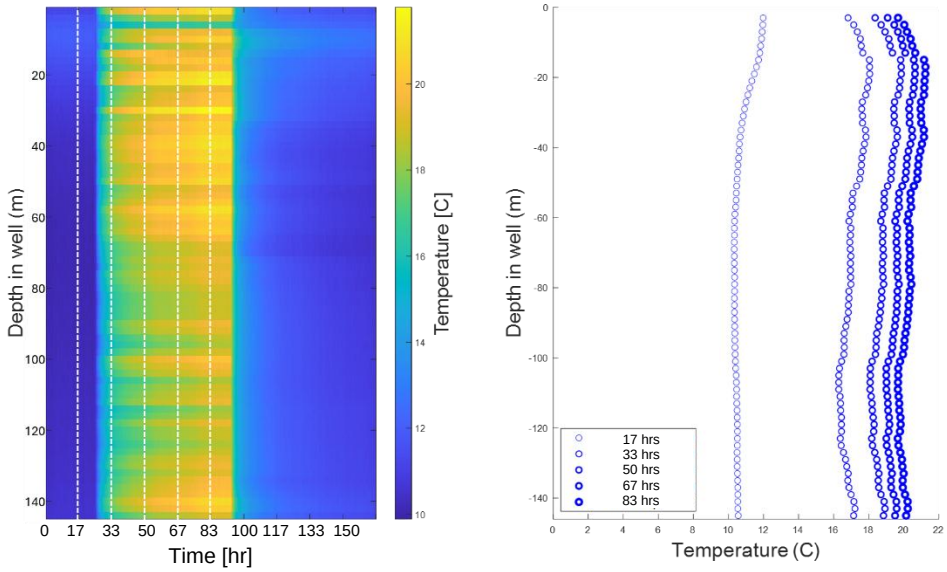

Figure 10: Waterfall plot and profile temperature in channel 1 during the C-TRT test.

5. ANALYSIS

A C-TRT was conducted at the West Point Annex site. Brightcore Energy completed the vertical bore on June 5, 2024. A Geothermal Resource Technologies (GRTI) test unit was attached to the vertical bore on the morning of June 17, 2024. Based on this conventional thermal response test, formation properties for Boring 1 were estimated as follows:

- Formation thermal conductivity = 2.82 W m^{-1} K^{-1} (1.63 BTU h^{-1} ft^{-1} °F^{-1})
- Formation thermal diffusivity = $1.13 \cdot 10^{-6}$ m^2 d^{-1} (1.06 ft^2 d^{-1})
- Bore thermal resistance = 0.125 m K W^{-1} (0.216 h ft °F BTU^{-1})

- Undisturbed formation temperature = 11.2 to 11.9 C (52.1 to 53.5 °F)

Two FO cables were installed at the site; one along the outside of an HDPE pipe running 304 m (1,000 ft) down the well and up the well, and another inside each leg of the HDPE pipe. Both cables were protected by 9.5-mm-diameter (3/8 in.) plastic tubing. Calibration of the temperature distribution was achieved by deploying cold and hot water baths, monitored with thermocouples, to refine the DTS system's accuracy (Figures 4-8). The DTS system consisted of four interrogator channels operating in a single-ended configuration. Calibration was enhanced by running the fibers through the water baths, providing contrasting temperature profiles to validate the DTS readings (Figures 2 and 3). The fiber cables, along with a DTS interrogator, were installed for D-TRT. This optical-based technique employs distributed temperature profiles to reconstruct the well's thermal history during and after the C-TRT (Figures 8 through 10).

Temperature data collected over time and depth (Figures 9 and 10) from these deployments contribute to understanding the well's thermal dynamics. We used the numerical derivative of temperature with depth, along with the power reported by the C-TRT, to estimate the local thermal conductivity of the different formation layers (McDaniel et al. 2018c). We use an analog model to evaluate the distributed hydraulic conductivity during a pumping test in a borehole to evaluate the thermal conductivity λ_k of the layer k within the formation:

$$\lambda_k = \frac{\frac{\Delta Q_{w,k}}{\Delta z_k}}{\frac{QP_w}{B}} \lambda_{ss} \tag{6}$$

where $\Delta Q_{w,k} = (T_2 - T_1) \cdot Q_w \cdot \rho_w \cdot C_{p,w}$ is the incremental heat flow into the layer k, $(T_2 - T_1)$ is the difference in temperature across layer k, ρ_w = 100 kg m^{-3} is the density of water, $C_{p,w}$ = 4184 J kg^{-1} K^{-1}is the heat capacity of water, Δz_k is the thickness of layer k, QP_w/B is the total water flow within the HDPE pipe over the depth of the pipe B, and λ_{ss} is the thermal conductivity reported by the C-TRT test. We report local 2-m-separated results by smoothing the data with a moving-average depth filter to remove noise introduced by the optical signal in the DTS response due to the calibration bath temperature, and to reduce the high-frequency increase introduced by the derivative operator in the numerator of equation 6. We also present segmental thermal conductivities for each layer using the slope of the temperature drop between the top and bottom of that layer. Results are presented in Figure 11.

Please note that the average thermal conductivity obtained from the C-TRT results is slightly larger than the segmental thermal conductivity based with the D-TRT results. These differences may be due to the reported noise. However, the use of DTS, along with C-TRT, allows evaluation of the formation's local thermal conductivity and should lead to a more rational design of commercial and district-scale geothermal fields, properly assessing thermal properties with depth.

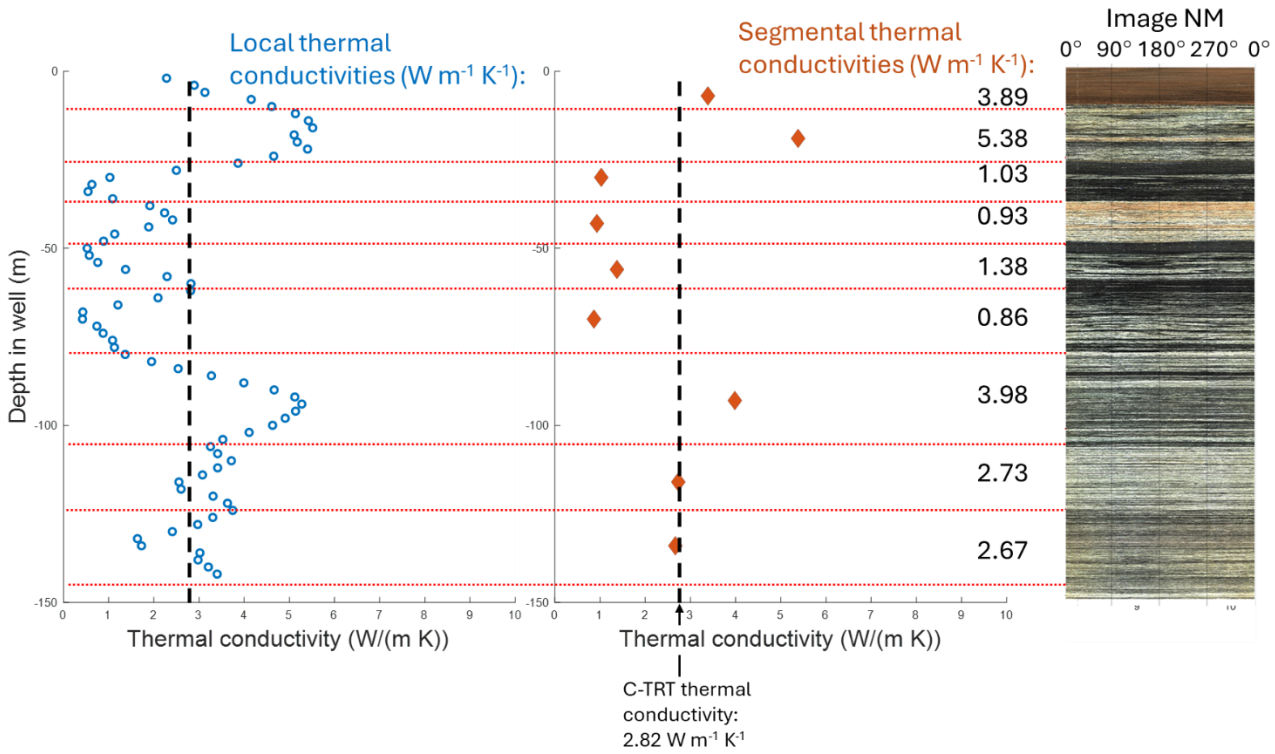

Figure 11: Thermal conductivity ranges for the test borehole at the West Point site based on the D-TRT results using the DTS data from inside the HDPE pipe. The dotted red lines indicate the layers determined from the D-TRT results. The blue circle shows the 2-m wide thermal conductivities, and the orange diamonds indicate the thermal conductivity values across layers. The dashed black lines indicate the average thermal conductivity value given by the C-TRT.

6. CONCLUSIONS

A subsurface investigation of three geothermal boreholes drilled in the Hudson Highlands region of New York State was conducted to determine the heat-transfer properties of the local bedrock for geothermal applications. The boreholes were drilled to varying depths and tested using a combination of field and laboratory techniques, including conventional Thermal Response Testing (C-TRT), geophysical logging, and mineralogical analysis. In this paper, the emphasis was on the value addition of Fiber-optic Distributed Thermal Response Testing (D-TRT). The overall objective was to assess lithology, hydrogeology, and thermal response behavior at these locations to aid the interpretation of distributed thermal response tests. Geophysical logs were collected to characterize subsurface conditions, with a particular focus on fluid properties, geological features, and fracture systems.

The bedrock encountered in the D-TRT geothermal borehole was primarily composed of gneiss and amphibolite, with variations in mineral composition. Gneiss layers contained quartz, feldspar, biotite, and hornblende, while amphibolite layers showed pyroxene and garnet. The thermal conductivity of these materials typically ranges between 1.7 and 5.7 W m^{-1} K^{-1} for gneiss and between 2.2 W m^{-1} $K^{-1}$and 2.7 W m^{-1} K^{-1} for amphibolite, depending on factors such as mineral content, water saturation, and fractures (Kavanaugh et al. 1997). Our D-TRT results indicated thermal conductivity values ranging from 0.86 to 5.38 W m^{-1} K^{-1}, which both support the variability of thermal properties in metamorphized rocks and their dependence on mineralogy, bedding dips, faulting, and other features. The C-TRT yielded a composite thermal conductivity of 2.82 W m^{-1} K^{-1}, consistent with the formation-weighted D-TRT results.

7. ACKNOWLEDGEMENTS

This project is part of the Federal Geothermal Partnerships (FedGeo) initiative. FedGeo partners with the United States Department of Energy's Office of Geothermal with the Federal Energy Management Program (FEMP) to help expand geothermal heating and cooling at federal sites nationwide. Parallel technical assistance efforts included resource assessments for ground- and mine-source geothermal exchange systems at Detroit Arsenal in Detroit, MI (Tinjum et al. 2026), and the Steward Shaft in Butte, MT (Kim et al. 2026). The FedGeo team provided data analysis, resource characterization, site surveys, and geothermal heat pump and/or geothermal district-scale system design options to the sites. This project was coordinated by technical leads at the National Laboratories that formed FedGeo, including Christine Doughty (Lawrence Berkeley National Laboratory), Xiaobing Liu (Oak Ridge National Laboratory), Matt Mitchell (National Laboratory of the Rockies), and Timothy Yoder (Pacific Northwest National Laboratory). Dr. Bass Shakra, Energy Manager for USAG West Point, provided invaluable site access, coordination, energy-related data, and logistics. Andrew Stumpf of the Illinois Geological Survey provided background and insight into the geological features at the West Point site. Alicia Luebbe and Nate Opperman, with Geological Engineering at UW–Madison, and Pete Chase, with the Wisconsin Geological and Natural History Survey, developed and collected field data. Without their support and teamwork, this project would not have been possible.

8. REFERENCES

American Society of Heating, Refrigerating and Air-Conditioning Engineers (ASHRAE): Geothermal Energy. In 2011, ASHRAE Handbook - HVAC Applications, 34, (2011).

Busby, J., Lewis, M., Reeves, H., and Lawley, R.: Initial geological considerations before installing ground source heat pump systems, Quarterly Journal of Engineering Geology and Hydrogeology, (2009), 42(3): 295–306. https://doi.org/10.1144/1470-9236/08-092

Catolico, N., Ge, S., and McCartney, J.S.: Numerical modeling of a soil-borehole thermal energy storage system, Vadose Zone Journal. 15(1), (2016), 1-17. https://doi.org/10.2136/vzj2015.05.0078

Chua, K., Chou, S.K., and Yang, W.M.: Advances in heat pump systems: a review, Applied Energy, 87, (2010), 3611–24. https://doi.org/10.1016/j.apenergy.2010.06.014

Clauser, C. and Huenges, E.: Thermal conductivity of rocks and minerals. In T. Ahrens, rock physics and phase relations-a handbook of physical constants, Washington: AGU reference shelf, 3(1080-305X), (1995), 105–126.

Dehkordi, S.E. and Schincariol, R.A.: Effect of thermal-hydrogeological and borehole heat exchanger properties on performance and impact of vertical closed-loop geothermal heat pump systems, Hydrogeology Journal, 22(1), (2013), 189–203. https://doi.org/10.1007/s10040-013-1060-6

Department of Energy: Research and Development Roadmap: Geothermal (Ground-Source) Heat Pumps, prepared by Goetzler, W., Guernsey, M., and Kar, R. for the U.S. Department of Energy, Building Technologies Program, (2012).

Diao, N., Li, Q., and Fang, Z.: Heat transfer in ground heat exchangers with groundwater advection, International Journal of Thermal Sciences, 43(12), (2004), 1203–1211. https://doi.org/10.1016/j.ijthermalsci.2004.04.009

Eskilson, P.: Thermal analysis of heat extraction boreholes. Ph.D. Thesis. University of Lund, Lund, Sweden, (1987).

Fan, R., Gao, Y., Pan, Y., and Zhang, Y.: Research on cool injection and extraction performance of borehole cool energy storage for ground coupled heat pump system, Energy and Buildings, 101, (2015), 35–44. https://doi.org/10.1016/j.enbuild.2015.05.006

Fan, R., Jiang, Y., Yao, Y., Shiming, D., Ma, Z.: A study on the performance of a geothermal heat exchanger under coupled heat conduction and groundwater advection, Energy, 32, (2007), 2199–2209. https://doi.org/10.1016/j.energy.2007.05.001

Grant, M.A., Donaldson, I.G., and Bixley, P.F.: Geothermal reservoir engineering, Academic Press, San Diego, California, (1982), 369 p.

Hecht-Méndez, J., Molina-Giraldo, N., Blum, P., Bayer, P.: Evaluating MT3DMS for heat transport simulation of closed geothermal systems, Groundwater. 48(5), (2010), 741–756. https://doi.org/10.1111/j.1745-6584.2010.00678.x

Heeg, E., Tinjum, J.M., Fratta, D., Attri, S.D., and Hart, D.J.: Seasonal Performance Evaluation for a District-Scale Geothermal Exchange System, 17th Pan-American Conference on Soil Mechanics and Geotechnical Engineering, La Serena, Chile, (2024).

Hellström, G.: Duct ground heat storage model: Manual for computer code, University of Lund, Lund, Sweden, (1989).

Horai, K. and Simmons, G.: Thermal conductivity of rock-forming minerals, Earth and Planetary Science Letters, 6(5), (1969), 359–368. https://doi.org/10.1016/0012-821X(69)90186-1

IGSHPA: Design and installation standards, International Ground Source Heat Pump Association, Stillwater, Oklahoma, (1991).

Isachsen, Y. W., Landing, E., Lauber, J. M., Rickard, L. V., and Rogers, W. B.: Geology of New York: A simplified Account (Second Edition). New York State Museum/Geological Survey, State Education Dept., University of the State of New York, (2000).

Johnson, M., and Gellasch, C.: Geology in the West Point, New York region and its influence on three centuries of local land use, Northeastern Geology and Environmental Geosciences, 26, (2004), 285–297.

Kim, J., Tinjum, J.M., Fratta, D., and Hart, D.J.: Measured Performance of a District-Scale Geothermal Heat Exchange System at Ground-Source and Building-Side, 51st Workshop on Geothermal Reservoir Engineering. Stanford University, Stanford, California, February 9-11, 2025, SGP-TR-230, (2026).

Knudson, R.: Energy Monitoring and Verification of Ground-Coupled Heat Pumps: Utilizing Live Building Control Data in the Wisconsin Institutes for Discovery, Master's Thesis, University of Wisconsin-Madison, (2013).

Liu, X., McCabe, K., and Spitler, J.: GeoVision Analysis Support Task Force Report: Thermal Applications—Geothermal Heat Pumps, ORNL/TM-2019/502, (2019).

McDaniel, A., Fratta, D., Tinjum, J., and Hart, D.: Long-term District-scale Geothermal Exchange Borefield Monitoring with Fiber Optic Distributed Temperature Sensing, Geothermics, 72C, (2018a), 193-204. https://doi.org/10.1016/j.geothermics.2017.11.008

McDaniel, A., Tinjum, J., Hart, D., and Fratta, D.: Dynamic Calibration for Permanent Distributed Temperature Sensing Networks, IEEE Sensors Journal. 18(6), (2018b), 2342-2352. https://doi.org/10.1109/JSEN.2018.2795240.

McDaniel, A., Tinjum, J., Hart, D. J., Lin, Y.-F., Stumpf, A., and Thomas, L.: Distributed thermal response test to analyze thermal properties in heterogeneous lithology. Geothermics. 76, (2018c), 116-124. http://doi.org/10.1016/j.geothermics.2018.07.003

Meyer, L.: Thermophysical properties of Wisconsin rocks for application in geothermal energy, Master's Thesis, University of Wisconsin-Madison, (2013)

NLR: National Laboratory of the Rockies – About, (2026). URL: https://www.nrel.gov/about [Accessed on January 2006].

O'Brien, L.E.: Geology Across the Great Valley - From the Shawangunks to the Hudson Highlands, in Waines, R. H., ed., New York State Geological Association, 59th annual meeting, Kingston, N.Y., Nov. 6-8, (1987), F-l-F-18. URL: https://ottohmuller.com/nysga2ge/Files/1987/NYSGA%201987%20F%20-%20Geology%20Across%20The%20Great%20Valley%20-%20From%20The%20Shawangunks%20To%20The%20Hudson%20Highlands.pdf [Accessed on January 2026].

Ozdogan-Dolcek, A., Tinjum, J.M., and Hart, D.J.: Numerical modeling of ground temperature response in a ground source heat pump system (GCHP), American Society of Civil Engineers (ASCE) Geo-Congress 2014 Technical papers, (2014), 2755-2766.

Ozenger, L., Hepbasli, A., and Dincer, I.: Effect of reference state on the performance of energy and exergy evaluation of geothermal district heating system: Balcova example, Build Environmental, 41, (2006), 699–709. https://doi.org/10.1016/j.buildenv.2005.03.007

Piipponen, K., Martinkauppi, A., Korhonen, K., Vallin, S., Arola, T., Bischoff, A., and Leppäharju, N. The deeper the better? A thermogeological analysis of medium-deep borehole heat exchangers in low-enthalpy crystalline rocks. Geothermal Energy, 10, (2022),1-20. https://doi.org/10.1186/s40517-022-00221-7.

Spitler, J.: Ground-source heat pump system research: past, present, and future. Heating, Ventilation, Air Conditioning, and Refrigeration Research, 11(2), (2005), 165–168. https://doi.org/10.1080/10789669.2005.10391132

Tinjum, J.M., Fratta, D., Hart, D.J., and Luebbe, A.: Optimizing the Geothermal Resource at the Detroit Arsenal, 51st Workshop on Geothermal Reservoir Engineering. Stanford University, Stanford, California, February 9-11, 2026. SGP-TR-230, (2026).

Walker, M.D., Meyer, L.L., Tinjum, J.M., and Hart, D.J.: Thermal property measurement of stratigraphic units with modeled implications for expected performance of vertical ground source heat pumps, Journal of Geological and Geotechnical Engineering. 33, (2015), 223–238. https://doi.org/10.1007/s10706-015-9847-y

Yang, T., Zhang, X.S., Zhou, B., and Zheng, M.: Simulation and experimental validation of soil cool storage with seasonal natural energy, Energy and Buildings, 63, (2013), 97–107. https://doi.org/10.1016/j.enbuild.2013.03.019

Yavuzturk, C.: Modeling of vertical ground loop heat exchangers for ground source heat pump systems, Oklahoma: Doctoral Thesis, Oklahoma State, (1999).

Zhou, P., Chen, C., Wu, J., Hu, G., Guo, Y., and Li, K.: Study on heat transport of soil thermal recovery of ground source heat pump system, in Proceedings of the 8th International Symposium on Heating, Ventilation and Air Conditioning. 2, (2014), 449–460. https://doi.org/10.1007/978-3-642-39581-9_45

Zimmerman, R., Thermal conductivity of fluid-saturated rocks, Journal of Petroleum Science and Engineering. 3, (1989), 219–227. https://doi.org/10.1016/0920-4105(89)90019-3